Results in Engineering 26 (2025) 104656

Contents lists available at ScienceDirect

Results in Engineering

journal homepage: www.sciencedirect.com/journal/results-in-engineering

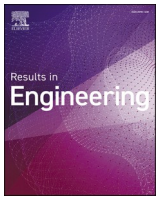

Research paper

Redox mediator system: Expanding the potential of laccase-like nanozymes towards pollutant remediation

E. Hermosilla [a,b,**], M. Diaz [a,b], M.J. Pérez-Vélez [c], S. Leiva [d], A.M.R. Ramírez [c,*], M.R.V. Lanza [e], O. Rubilar [a,b]

[a] Biotechnological Research Center Applied to the Environment (CIBAMA), Universidad de La Frontera, Temuco 4811230, Chile
[b] Departamento de Ingeniería Química, Universidad de La Frontera, Temuco 4811230, Chile
[c] Departamento de Ciencias Químicas y Recursos Naturales, Facultad de Ingeniería y Ciencias, Universidad de La Frontera, Temuco 4811230, Chile
[d] Estudiante Ingeniería Civil Química, Departamento de Ingeniería Química, Facultad de Ingeniería y Ciencias, Universidad de La Frontera, Temuco 4811230, Chile
[e] Intitute of Chemistry of São Carlos, University of São Paulo, São Carlos, SP 13566-590, Brazil

ARTICLE INFO

Keywords:
Nanozyme
Laccase-like
Remediation
Redox mediators
Synergism

ABSTRACT

This study investigates the use of a redox mediator system to enhance the pollutant remediation capabilities of laccase-like nanozymes. A three-phase magnetic nanocomposite, composed of $MnFe_2O_4$, Mn_3O_4, and CuO in various precursor ratios, was synthesized. The 1:2:2 nanocomposite demonstrated the highest specific laccase-like activity, with values of 8.9 U mg^{-1} at pH 4 and 9.2 U mg^{-1} at pH 5. In contrast, single-phase nanozymes exhibited much lower activities. Cyclic voltammetry (CV) revealed that the 1:2:2 composite had a $MnFe_2O_4$ core and a Mn_3O_4|CuO alloy shell. The study also evaluated natural and synthetic redox mediators—acetosyringone, syringaldehyde, vanillin, and 1-hydroxybenzotriazole (HBT)—for their effect on methyl orange degradation. Acetosyringone was the most effective, achieving near-complete degradation at 50 μM and above, resulting in a 6.3-fold increase in degradation rate compared to treatments without mediators. Syringaldehyde and vanillin also enhanced degradation, with syringaldehyde reaching near-complete degradation at 75 μM and 100 μM, while vanillin required higher concentrations for 80 % degradation. CV was used to analyze the electrochemical properties of reactions involving the 1:2:2 nanocomposite and redox mediators. These findings highlight the potential of combining nanozymes with natural redox mediators for improved degradation of harmful compounds in environmental remediation. While laccase-like nanozymes have typically been used for sensor applications, this study opens new possibilities for their use in environmental challenges and catalytic systems.

1. Introduction

Laccase is one of the most researched and versatile enzymes for the wastewater treatment and degradation of several compounds that can be found in the effluents from industries and hospitals, including herbicides, fertilizers, synthetic dyes, polycyclic aromatic hydrocarbons (PAH), chlorinated paraffin phthalates, and emerging pollutants, which may include pharmaceuticals (antibiotics, hormones, endocrine disruptors), plasticizers, and compounds derived from self-care products, among others [1–5]. Laccase catalyzes non-specific oxidation of a wide range of substrates, particularly substituted phenols and aromatic amines, converting them into unstable radicals using oxygen as an electron acceptor and generating water as a by-product [6]. These unstable compounds generated free radicals initiate cascade reactions, leading to chemical transformations that can reach the complete substrate mineralization into carbon dioxide and water [1]. However, laccases have a redox potential ranging from 0.5 to 0.8 V [7,8], which is less than that of peroxidases (1.1 to 1.26 V) [9]. Several studies have demonstrated the effectiveness of a redox mediator system to enhance the redox potential of laccase for degrading compounds. This strategy involves the utilization of phenolic compounds, functioning as redox mediators, to serve as intermediaries between laccase and the targeted pollutant. By facilitating electron transfer processes, these mediators enhance the breakdown process, resulting in degradation rates that can increase by 20 to 80 % [10,11]. While laccase and other natural enzymes have shown remarkable efficiency in degrading a wide range of

* Corresponding author.
** Corresponding author at: Biotechnological Research Center Applied to the Environment (CIBAMA), Universidad de La Frontera, Temuco 4811230, Chile.
E-mail addresses: edward.hermosilla@ufrontera.cl (E. Hermosilla), andres.ramirez@ufrontera.cl (A.M.R. Ramírez).

https://doi.org/10.1016/j.rineng.2025.104656
Received 11 September 2024; Received in revised form 7 January 2025; Accepted 16 March 2025
Available online 17 March 2025

environmental pollutants, they face several limitations that hinder their broader application in real-world wastewater remediation systems. Natural enzymes, including laccase, often exhibit poor stability under diverse environmental conditions, such as extreme pH, high temperatures, or the presence of inhibitors commonly found in industrial effluents [12,13]. These limitations significantly reduce their catalytic efficiency and lifespan, necessitating frequent enzyme replacement and increasing the operational costs. Additionally, the production of natural enzymes remains costly and resource-intensive, as it often involves laborious purification steps and the maintenance of strict growth conditions for producing microbial or fungal strains [14]. Conversely, nanozymes, which are engineered nanomaterials designed to emulate the catalytic activities of natural enzymes, present an innovative alternative. These nanozymes, including materials such as Fe_2O_3, Pt, Fe-Pt, Ag_2O, Tb_2O_7, Au/Pt, Pt-Se, Mn_3O_4, MnO_2, CuO, CeO_2, $MnFe_2O_4$, as well as metal-organic frameworks (MOF), exhibit enzyme-like activities including those akin to peroxidase, oxidase, laccase, and catalase [15–23]. Nanozymes provide several advantages compared to natural enzymes, including cost-effective production, enhanced chemical stability, and the ability to control their shape, size, composition, and surface characteristics. Additionally, the magnetic properties of ferrite nanozymes enable easy reuse, facilitating the development of these materials with technological scalability and potential for industrial applications [24]. Similar approaches have been reported for natural laccase immobilized on magnetic nanomaterials as supports [25–27]. Furthermore, the catalytic application of nanoparticles with laccase-like activity has been predominantly restricted to detection methods that involve the oxidation of easily oxidizable substrates [23,28–31], rather than compounds requiring enzymes with higher redox potentials, such as synthetic dyes. To date, the effect of redox mediators on the activity of nanozymes has not been thoroughly explored.

This study aimed to synthesize a nanozyme based on a ternary heterostructure composed of $MnFe_2O_4$, Mn_3O_4, and CuO, materials that have been reported to exhibit laccase-like activity. We expected to enhance this activity through the synergistic effect of combining these materials. The incorporation of $MnFe_2O_4$ also confers magnetic properties to the nanozyme, facilitating its recovery and reuse using an external magnetic field. Besides, we evaluated the influence of natural redox mediators (acetosyringone, syringaldehyde and vainillin) on the catalytic activity of nanozymes for degrading methyl orange as a model azo-dye compound (Fig. 1). Additionally, the electrochemical characteristics of the reaction between redox mediators and the nanozyme were studied to understand and compare the mechanisms of the nanozyme with those of natural laccase reported in the literature.

2. Methodology

2.1. Reagents

The reagents, methyl orange (MO), hexadecyltrimethylammonium bromide (CTAB), the enzymatic substrates (3-Methyl-2-benzothiazolinone hydrazone (MBTH), 1.5 mM 4-(Dimethylamino)benzaldehyde (DMAB), and 2,2′-azino-bis(3-ethylbenzothiazoline-6-sulfonic acid) (ABTS)), redox mediators (acetosyringone, syringaldehyde, vainillin and 1-hydroxybenzotriazole) were purchased from Merck (Darmstadt, Germany).

2.2. Synthesis of $MnFe_2O_4$ nanozymes

The synthesis of $MnFe_2O_4$ nanozymes was carried out using the co-precipitation method, as described by Hermosilla et al. [22]. Initially, 17 mL of 7 M NaOH solution was placed in a 250 mL glass flask and heated to 90 °C in a glycerin bath. Mechanical stirring was maintained at 400 rpm throughout the synthesis process. A mixture comprising 2.25 mL of 4 M $FeCl_3$, 2.25 mL of 2 M $MnCl_2$, and 22.5 mL of ultrapure water was then added dropwise to the flask at a rate of 2 mL min^{-1}, employing a peristaltic pump for controlled delivery. Following this, a combination of 1 mL of CTAB (as stabilizing agent) at a concentration of 4.6 mg mL^{-1} and 1 mL of 3 mg mL^{-1} NH_4Cl was introduced into the reaction mixture through a peristaltic pump, also at a rate of 2 mL min^{-1}. The mixture was continuously stirred and maintained at a constant temperature of 90 °C for 2 h to ensure the completion of the reaction. This process resulted in the formation of a dark brown precipitate, which was subsequently washed three times with water to remove the reagent excess.

2.3. Synthesis of Mn_3O_4 nanozymes

The Mn_3O_4 nanozymes were synthesized utilizing a chemical precipitation method. Initially, 25 mL of a 0.5 M NaOH solution was introduced into a 250 mL reaction flask, which was subsequently heated to 90 °C in a glycerin bath. Following this step, 25 mL of a 0.2 M $MnSO_4$ solution, along with 51 mg of CTAB, were incrementally added to the flask at a controlled rate of 2 mL min^{-1} using a peristaltic pump. This step was followed by the addition of 2 mL of 30 % hydrogen peroxide to the mixture, also at a rate of 2 mL min^{-1}. The reaction mixture was subjected to continuous agitation at a stable temperature of 90 °C for 2

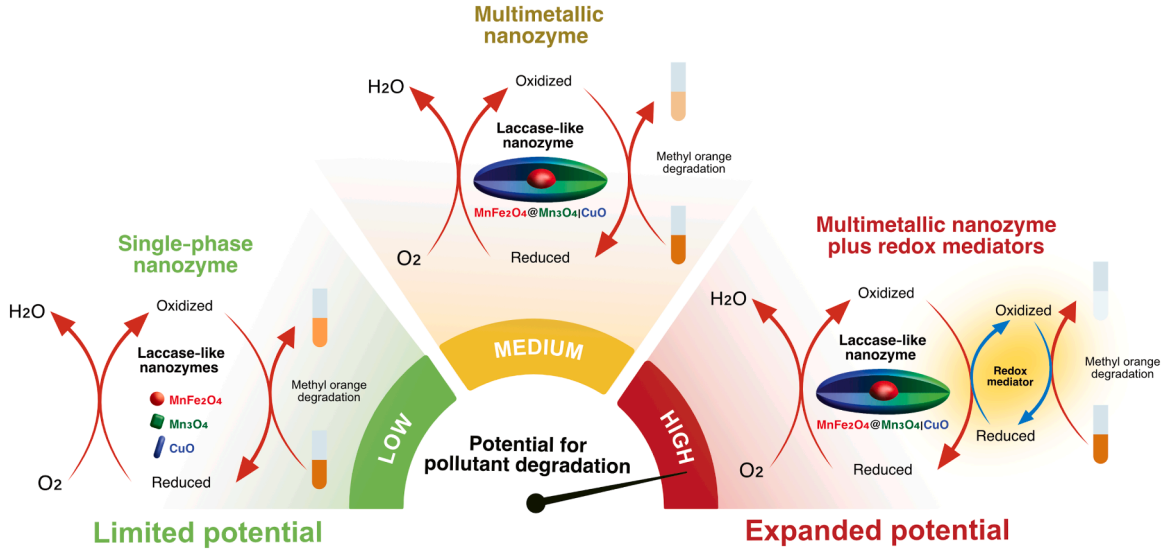

Fig. 1. Schematic illustration representing the key steps involved in enhancing the laccase-like activity of metal oxide nanozymes as evaluated in this study.

h. Subsequently, the formed nanozymes were recovered from the reaction mixture through centrifugation at 4300 rpm, followed by triple washing with distilled water to eliminate any residual reactants.

2.4. Synthesis of CuO nanozymes

The CuO nanozymes were synthesized utilizing the sol-gel method [32]. The synthesis commenced with the preparation of a reaction mixture in a 250 mL glass flask; this mixture comprised 50 mL of a 0.1 M $CuSO_4$ solution and 51 mg of CTAB. The flask was placed on a heating plate submerged in a glycerin bath, with the temperature maintained at 90 °C. A vertical homogenizer, set at 500 rpm, was used to ensure uniform mixing. Following the initial setup, 17 mL of 0.5 M NaOH solution was added gradually to the flask at a controlled rate of 2 mL min^{-1}, facilitated by a peristaltic pump. The reaction was continuously agitated at 90 °C for 2 h to ensure complete synthesis. Afterward, the mixture was subjected to vacuum filtration to separate the precipitated nanozymes. The collected precipitate was then washed three times with water to remove any unreacted substances or residual reactants.

2.5. One-pot synthesis of $MnFe_2O_4/Mn_{3O4}$ nanozymes

The $MnFe_2O_4/Mn_3O_4$ two-phase nanozymes were synthesized using various molar ratios of Mn:Mn (1:1) to evaluate their effect on Laccase-like activity. Synthesis was performed in round-bottom flasks, which were mechanically stirred at 400 rpm on a heating plate within a glycerin bath maintained at 90 °C. Briefly, 17 mL of a 7 M NaOH solution was added to the flask, which was subsequently heated to 90 °C and sealed with a rubber stopper. Following this, a solution containing 25 mL of $FeCl_3{\cdot}6H_2O$ and $MnCl_2$ was added using a peristaltic pump at a flow rate of 2 mL min^{-1}, achieving final concentrations of 0.2 M for Fe^{3+} and 0.1 M for Mn^{2+}. Afterward, 1 mL of CTAB and 1 mL of NH_4Cl were added at the same flow rate. The reaction mixture was kept under constant agitation and temperature for 2 h. Then, a solution of 10 mL of $MnSO_4{\cdot}4H_2O$ was added dropwise at 2 mL min^{-1} to reach a final Mn^{2+} concentration of 0.1 or 0.2 M in the mixture for each specific molar ratio, followed by the addition of 4 mL of H_2O_2 at the same rate. These conditions were maintained for an additional 2 h. The resulting precipitate was separated using a neodymium magnet and washed three times with deionized water.

2.6. One-pot synthesis of $MnFe_2O_4/CuO$ nanozymes

The $MnFe_2O_4/CuO$ two-phase nanozymes were synthesized using various molar ratios of Mn:Cu (1:1) to evaluate their effect on Laccase-like activity. Synthesis was performed in round-bottom flasks, which were mechanically stirred at 400 rpm on a heating plate within a glycerin bath maintained at 90 °C. Briefly, 17 mL of a 7 M NaOH solution was added to the flask, which was subsequently heated to 90 °C and sealed with a rubber stopper. Following this, a solution containing 25 mL of $FeCl_3{\cdot}6H_2O$ and $MnCl_2$ was added using a peristaltic pump at a flow rate of 2 mL min^{-1}, achieving final concentrations of 0.2 M for Fe^{3+} and 0.1 M for Mn^{2+}. Afterward, 1 mL of CTAB and 1 mL of NH_4Cl were added at the same flow rate. The reaction mixture was kept under constant agitation and temperature for 2 h. Subsequently, 10 mL of $CuSO_4{\cdot}5H_2O$ solution was introduced at a flow rate of 2 mL min^{-1} to achieve a final Cu^{2+} concentration of 0.1 or 0.2 M, and the reaction was continued for another 2 h. The resulting precipitate was separated using a neodymium magnet and washed three times with deionized water.

2.7. One-pot synthesis of three-phase nanozymes

The $MnFe_2O_4/Mn_3O_4/CuO$ three-phase nanozymes were synthesized using various molar ratios of Mn:Mn:Cu (1:1:1, 2:1:1, 1:2:1, 1:1:2, 2:2:1, 2:1:2, 1:2:2) to evaluate their effect on Laccase-like activity. Synthesis was performed in round-bottom flasks, which were mechanically stirred at 400 rpm on a heating plate within a glycerin bath maintained at 90 °C. Briefly, 17 mL of a 7 M NaOH solution was added to the flask, which was subsequently heated to 90 °C and sealed with a rubber stopper. Following this, a solution containing 25 mL of $FeCl_3{\cdot}6H_2O$ and $MnCl_2$ was added using a peristaltic pump at a flow rate of 2 mL min^{-1}, achieving final concentrations of 0.2 M for Fe^{3+} and 0.1 M for Mn^{2+}. Afterward, 1 mL of CTAB and 1 mL of NH_4Cl were added at the same flow rate. The reaction mixture was kept under constant agitation and temperature for 2 h. Then, a solution of 10 mL of $MnSO_4{\cdot}4H_2O$ was added dropwise at 2 mL min^{-1} to reach a final Mn^{2+} concentration of 0.1 or 0.2 M in the mixture for each specific molar ratio, followed by the addition of 4 mL of H_2O_2 at the same rate. These conditions were maintained for an additional 2 h. Subsequently, 10 mL of $CuSO_4{\cdot}5H_2O$ solution was introduced at a flow rate of 2 mL min^{-1} to achieve a final Cu^{2+} concentration of 0.1 or 0.2 M, and the reaction was continued for another 2 h. The resulting precipitate was separated using a neodymium magnet and washed three times with deionized water.

2.8. Characterization of nanozymes

The synthesized nanozymes were characterized using a suite of analytical techniques to understand their structure, morphology, and magnetic features. X-ray diffraction (XRD) analysis of nanozymes was carried out in a Bruker D8 Advance diffractometer (40 kV/30 mA Cu Kα radiation) with LynxEye linear detector (Bruker, Karlsruhe, Germany), while transmission electron microscopy (TEM) was carried out in a TEM JEOL 1200 EX II (JEOL Ltd, Tokyo, Japan).

2.9. Laccase-like activity

The laccase-mimicking activity of the synthesized nanozymes was assessed using two substrates: MBTH-DMAB and ABTS. In the MBTH-DMAB assay, the oxidation kinetics were determined in a cuvette (1-cm light path) filled with a reaction mixture comprising 100 μL of MBTH (14 mM), 300 μL of DMAB (6.6 mM), 400 μL of buffer, 450 μL of distilled water and 50 μL of the nanozyme solution in deionized water. The reaction kinetics were monitored by measuring the increase in absorbance at 590 nm (molar extinction coefficient of 53,000 M^{-1} cm^{-1}) at 1-second intervals for 2 min [22]. For the ABTS assay, the reaction was carried out in a cuvette (1-cm light path) with 400 μL of buffer, 100 μL of ABTS (15 mM), 950 μL of distilled water, and 50 μL of the nanozyme dispersion. This reaction was also conducted at 30 °C, monitoring the increase in absorbance at 420 nm using a molar extinction coefficient of 36,000 M^{-1} cm^{-1}. The effect of pH on these reactions was evaluated using acetate buffer (100 mM) for adjustments within a pH range of 3.0–5.0, and phosphate buffer (100 mM) for a pH range of 6.0–8.0 [33]. Spectrophotometric measurements were performed using a UV–Vis Spectroquant Prove 300 spectrophotometer (Merck KGaA, Darmstadt, Germany). Laccase-like activity was quantified by defining one unit (U) of activity as the amount of nanozyme necessary to oxidize one micromole of substrate per minute. For comparative analysis, the specific activity was reported in units per milligram (U mg^{-1}) of nanozymes, following the methodology of [34].

2.10. Assays of MO degradation by nanozyme-redox-mediator system

The degradation assays of methyl orange (MO) were conducted in Erlenmeyer flasks, employing specific concentrations of 20 mg L^{-1} MO and nanozyme concentrations of 50 and 100 mg L^{-1}, within a pH range of 4 and 5. These conditions were maintained for 1 hour at a constant shaking of 200 rpm. The extent of MO degradation was determined at a wavelength of 463 nm, utilizing a UV–Vis Spectroquant Prove 300 spectrophotometer for the measurement. The influence of various redox mediators—namely syringaldehyde, acetosyringone, vanillin, and 1-hydroxybenzotriazole —was assessed. These mediators were tested at final concentrations ranging from 25 to 100 μM, under identical

experimental conditions. Additionally, control treatments were performed, where the nanozyme was tested without redox mediators (no-mediator treatment) and where the redox mediators were tested without the nanozyme. All treatments were performed in triplicate, and the data are presented as the mean ± standard deviation of the results.

2.11. Recovery and recycling of nanozymes

The reutilization of nanozymes for MO degradation was assessed by conducting degradation assays in Erlenmeyer flasks containing 20 mg L^{-1} MO, 100 mg L^{-1} nanozyme, and 100 μM acetosyringone at pH 5. The reactions were incubated at 200 rpm for 1 hour. Afterwards, the nanozymes were magnetically recovered using a neodymium magnet, washed with distilled water, and reused in subsequent degradation cycles under identical conditions. The degradation efficiency and stability of the nanozymes were evaluated over seven consecutive cycles, with the data presented as the mean ± standard deviation of triplicates. Additionally, the metal ions released after each degradation cycle were measured using Total Reflection X-Ray Fluorescence (TXRF) spectroscopy. The analysis was carried out with a high-efficiency S4 T-STAR module (Bruker Nano GmbH, Berlin, Germany) equipped with a molybdenum (Mo) X-ray tube. Sample excitation was conducted at a voltage of 50 kV and a current of 1000 μA. The measurement time was set to 600 s. The evaluation of the obtained spectra was performed using Spectra PicoFox software (version 7.2.5.0, Bruker Nano GmbH).

2.12. Cyclic voltammetry

The electrochemical perturbations were performed through a CHI-920D potentiostat/galvanostat using a three-compartment cell with an Ag/AgCl reference electrode, a platinum wire as counter-electrode with a geometrical area 20 times larger than the glassy carbon electrode (GC) (3.0 mm diameter), used as the working electrode. Cyclic voltammetry was performed between −1.00 and 1.00 V, with a sweep speed, n,

$n = 0.05\ V\ s^{-1}$. The solution consisted of an acetate buffer at pH 4.0, where the different mediator groups (acetosyringone and syringaldehyde) and the nanozyme were added, with a concentration of each mediator of 50 mM and a nanostructure of 50 mg L^{-1}. All experiments were performed at room temperature.

3. Results and discussion

3.1. Laccase-like activity of nanozymes

The laccase-like activity of various metal oxide composites and their individual components under different pH conditions was spectrophotometrically evaluated using MBTH/DMAB and ABTS as substrates. The obtained results show the influence of nanozyme composition, precursor molar ratios, and pH on catalytic performance. Fig. 1a shows the specific laccase-like activity using MBTH/DMAB as the substrate. Among the single-phase materials, Mn_3O_4 exhibits the highest activity (1.74 U mg^{-1} at pH 3), followed by $MnFe_2O_4$ (0.26 U mg^{-1} at pH 4), and CuO (0.006 U mg^{-1} at pH 6). To synthesize magnetic nanozymes, $MnFe_2O_4$ phase was included in the synthesis of both two-phase and three-phase composites. To identify potential synergistic effect as "synergism factor" between metal oxide phase on the laccase-like activity, the theoretical activity of two and three-phase nanozymes was estimated using the following equation:

$$A_t = \frac{\sum_i (R_i \times A_i)}{\sum_i R_i}$$

Where, A_t is the theoretical activity of the combined material, R_i is the molar ratio of precursor in the combined material, A_i is the activity of precursor (i.e., the activity of the corresponding single-phase nanozyme), $\sum_i (R_i \times A_i)$ the sum of the weighted activities of each precursor, and $\sum_i R_i$ the sum of the molar ratios of all the precursors.

The synergism factor was calculated as the observed activity divided by the theoretical activity. A synergism factor greater than 1 indicates positive synergy, where the combined effect of components is greater than the sum of their individual effects. A value equal to 1 indicates an additive effect, meaning the components work independently without enhancing each other. A value <1 indicates antagonism, where the combined effect is less than expected. The $MnFe_2O_4|Mn_3O_4$ composites exhibited higher activity than $MnFe_2O_4$ alone but significantly lower activity compared to theoretical activity (Table 1). The $MnFe_2O_4|CuO$ composite showed lower activity than $MnFe_2O_4$ alone, indicating an antagonism effect between $MnFe_2O_4$ and CuO phases. By contrast, in the case of three-phase composites ($MnFe_2O_4@Mn_3O_4|CuO$), significantly higher activity was observed across all tested pH levels (pH 3, 4, and 5) compared to single-phase nanozymes and their estimated theoretical activities. All synthesized three-phase nanozymes shower a synergism effect with synergism index between 1.34 to 14.42. The composite with a precursor molar ratio of 1:2:2 reached the highest specific laccase-like activity of 8.9 U mg^{-1} and 9.2 U mg^{-1} at pH 4 and 5, respectively. This nanozyme exhibited a synergism factor of 14.4 relative to the theoretical activity, suggesting a synergistic effect among $MnFe_2O_4$, Mn_3O_4, and CuO that enhances catalytic performance. A comparative overview of the specific activities of three-phase nanozymes indicates that equimolar combinations of Mn_3O_4 and CuO precursors significantly enhance laccase-like activity. Conversely, increasing the proportion of $MnFe_2O_4$ in the composite synthesis results in diminished catalytic activity. However, the $MnFe_2O_4$ phase imparts magnetic properties to the nanozyme, facilitating its recovery and easy reuse after the catalytic process. The laccase-like activity measured using ABTS as the substrate shows a similar trend (Fig. 2b). The three-phase composite $MnFe_2O_4@Mn_3O_4|CuO$ consistently exhibits the highest activity across all pH levels, with the 1:2:2 ratio demonstrating superior performance. However, in most measurements using ABTS, the activity of the nanozymes was significantly higher at pH 4 compared to pH 5. Additionally, it was observed that the synthesized nanozymes have a higher affinity for ABTS compared to MBTH/DMAB, as indicated by the higher specific activity values when using ABTS. In both substrates, the activity generally decreases with lowering pH, suggesting that the catalytic performance is pH-dependent, with optimal activity at pH levels between 4 and 5. Composite nanozymes, such as $MnFe_2O_4|Mn_3O_4$ and $MnFe_2O_4|CuO$, also show varied activity, with $MnFe_2O_4|Mn_3O_4$ performing significantly better than $MnFe_2O_4|CuO$. The mixtures of nanozymes (1:1:1, 1:2:1, etc.) show notable variations in activity, with the 1:1:1 mixture displaying exceptionally high activity at all pH levels, particularly at pH 5 Table 2.

3.2. Chemical and morphological characterization of nanozymes

The Fig. 3a–d shows the X-ray diffraction (XRD) patterns which provide valuable insights into the structural properties of single-phase nanozymes and the three-phase 1:2:2 nanozyme. The XRD pattern for $MnFe_2O_4$ exhibits sharp and well-defined peaks, indicative of its high crystallinity and confirming the phase purity with a spinel structure. Similarly, the Mn_3O_4 pattern shows well-resolved peaks matching its tetragonal structure, confirming its high crystallinity and purity. The CuO pattern displays sharp peaks typical of its monoclinic structure, indicating high-purity and well-crystalline CuO. In the composite pattern of $MnFe_2O_4@Mn_3O_4|CuO$, a combination of peaks from all three oxides is evident, indicating that the composite retains the crystalline structures of $MnFe_2O_4$, Mn_3O_4, and CuO without significant peak shifts. This suggests no strong interactions or new phases formed among the oxides, highlighting the successful integration of these materials in the nanocomposite 1:2:2. The sharp peaks in all patterns confirm high crystallinity for both the individual oxides and the composite, which is desirable as it influences the material's physical properties, such as magnetic behavior, catalytic activity, and electronic performance. The

Table 1
Laccase-like activity using MBTH/DMAB (as the substrate) and synergism factor of the synthesized nanozymes at different pH levels.

Nanozyme		Laccase-like activity (U mg^{-1})						Synergism index		
		Experimental activity			Theoretical activity					
		pH 3	pH 4	pH 5	pH 3	pH 4	pH 5	pH 3	pH 4	pH 5
$MnFe_2O_4$		0.25	0.26	0.19	–	–	–	–	–	–
Mn_3O_4		1.74	1.70	1.49	–	–	–	–	–	–
CuO		0.001	0.002	0.006	–	–	–	–	–	–
$MnFe_2O_4$|Mn_3O_4		0.32	0.37	0.25	0.99	0.98	0.84	0.32	0.38	0.30
$MnFe_2O_4$|CuO		0.02	0.05	0.04	0.12	0.13	0.10	0.16	0.38	0.41
$MnFe_2O_4$@Mn_3O_4|CuO	1:1:1	5.70	5.17	6.73	0.66	0.65	0.56	*8.59	*7.91	*11.98
	1:2:1	2.53	2.45	3.67	0.93	0.92	0.79	*2.71	*2.68	**4.62
	1:1:2	0.88	1.13	1.30	0.66	0.71	0.70	*1.34	*1.59	*1.86
	1:2:2	6.79	8.90	9.18	0.75	0.73	0.64	**9.10	**12.15	**14.42
	2:1:1	1.99	1.57	2.16	0.56	0.56	0.47	*3.55	*2.83	**4.61
	2:1:2	1.09	1.13	1.03	0.78	0.79	0.71	*1.39	*1.43	*1.45
	2:2:1	1.32	1.51	3.18	0.79	0.78	0.67	*1.66	*1.93	**4.72

The synergism factor was calculated as the observed activity divided by the theoretical activity. An index greater than 1 indicates positive synergy (* and ** values), equal to 1 indicates an additive effect, and <1 indicates antagonism.

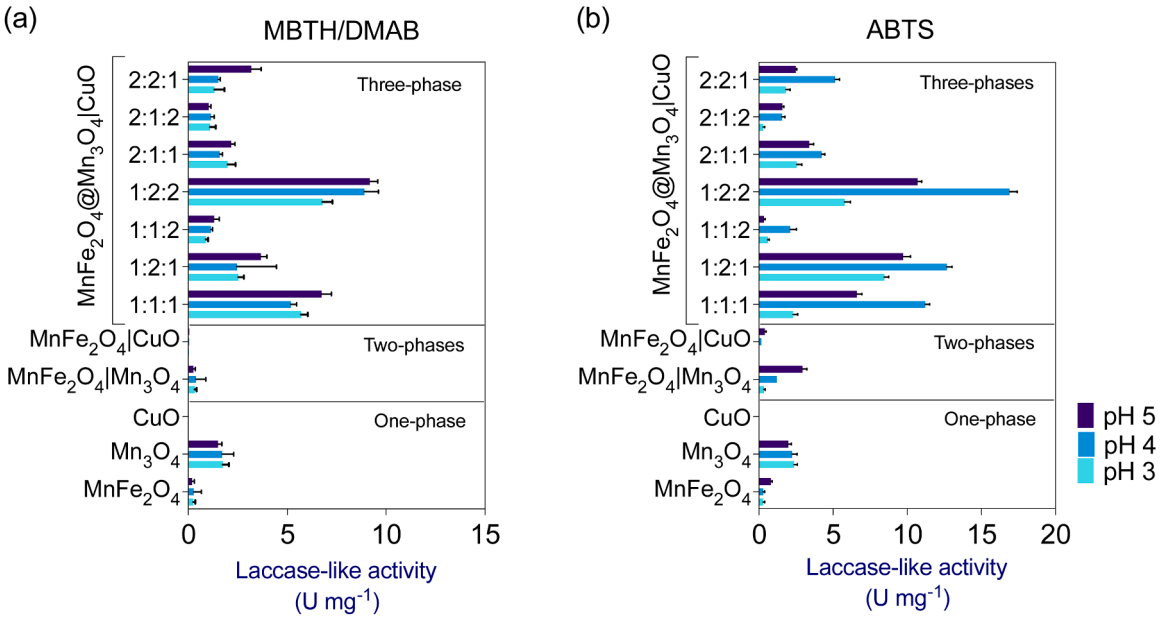

Fig. 2. Laccase-like specific activity (U mg^{-1}) of synthesized nanozymes assayed using (a) MBTH-DMAB and (b) ABTS substrates under acidic pH values 3 to 5. The data presented represent the mean values with standard deviations ($n = 3$).

Table 2
Laccase-like activity using ABTS (as the substrate) and synergism factor of the synthesized nanozymes at different pH levels.

Nanozyme		Laccase-like activity (U mg^{-1})						Synergism factor		
		Experimental activity			Theoretical activity					
		pH 3	pH 4	pH 5	pH 3	pH 4	pH 5	pH 3	pH 4	pH 5
$MnFe_2O_4$		0.79	0.28	0.28	–	–	–	–	–	–
Mn_3O_4		1.97	2.24	2.37	–	–	–	–	–	–
CuO		0	0.01	0.01	–	–	–	–	–	–
$MnFe_2O_4$|Mn_3O_4		2.93	1.21	0.31	1.38	1.26	1.32	*2.12	0.96	0.23
$MnFe_2O_4$|CuO		0.37	0.14	0.00	0.39	0.14	0.14	0.94	0.97	0.00
$MnFe_2O_4$@Mn_3O_4|CuO	1:1:1	6.59	11.21	2.31	0.92	0.84	0.89	*7.16	*13.29	2.61
	1:2:1	9.72	12.68	8.45	1.18	1.19	1.26	**8.22	**10.63	**6.72
	1:1:2	0.31	2.11	0.59	0.57	1.09	0.74	0.54	*1.93	0.79
	1:2:2	10.7	16.9	5.77	0.95	0.96	1.01	**11.31	**17.68	**5.72
	2:1:1	3.38	4.23	2.54	0.89	0.70	0.73	*3.81	**6.02	*3.46
	2:1:2	1.58	1.55	0.28	1.03	1.07	0.59	*1.54	*1.45	0.47
	2:2:1	2.48	5.13	1.80	1.10	1.01	1.06	*2.25	**5.08	*1.69

The synergism factor was calculated as the observed activity divided by the theoretical activity. An index greater than 1 indicates positive synergy (* and ** values), equal to 1 indicates an additive effect, and <1 indicates antagonism.

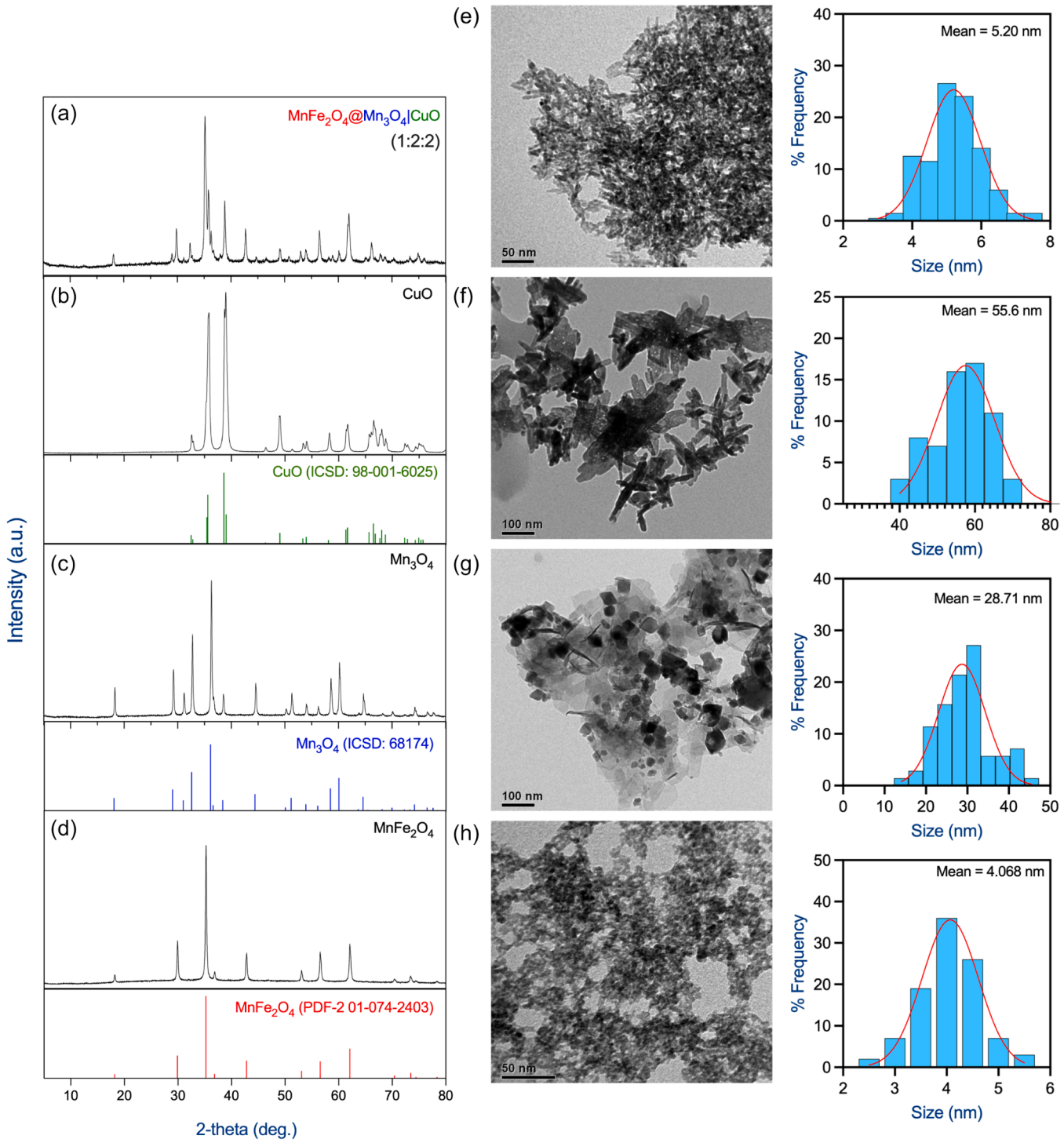

Fig. 3. (a-d) XRD patterns and (e-h) TEM images with corresponding size histograms of the synthesized nanozymes.

absence of additional peaks in the composite's XRD pattern suggests no new phases formed during nanocomposite synthesis, indicating good phase compatibility among $MnFe_2O_4$, Mn_3O_4, and CuO. This compatibility is crucial for maintaining the desirable properties of each oxide in the composite material. The XRD analysis confirms that the composite material is effectively composed of $MnFe_2O_4$, Mn_3O_4, and CuO, each retaining its crystalline structure. The one-pot synthesis process has successfully integrated these oxides without forming new phases. Quantitative phase analysis of XRD data using the Rietveld method yielded the following mass fractions for the 1:2:2 nanozyme: $MnFe_2O_4$ – 13.2 wt% (reference code 01–074–2403 from PDF-2), Mn_3O_4 – 45.5 wt% (ICSD: 68,174), and CuO – 41.3 wt% (ICSD 98–001–6025). The atomic composition is 35.9 % Mn, 32.9 % Cu, 24.7 % O, and 6.4 % Fe.

Transmission electron microscopy (TEM) images revealed that the synthesized single-phase nanozymes have distinct sizes and morphologies (Fig. 3e–h). The synthesized $MnFe_2O_4$ nanozymes exhibited a spherical shape with a mean size of 4.1 nm and a normal size distribution. The Mn_3O_4 nanozymes displayed a cubic shape with a mean size of 25.7 nm, while the CuO nanozymes exhibited a rod shape with a length of 55.6 nm. Additionally, the 1:2:2 composite exhibited a rod shape with a mean length of 5.2 nm and a normal size distribution. These results indicate that the synthesis method successfully produces nanozymes

with well-defined shapes and sizes, which are crucial for their catalytic properties. The spherical morphology of $MnFe_2O_4$ and the cubic structure of Mn_3O_4 suggest a high degree of crystallinity and uniformity, which are beneficial for consistent catalytic performance. The rod-shaped CuO and 1:2:2 composite nanozymes, with their larger aspect ratios, may offer enhanced surface area for catalytic reactions. These distinct morphologies and sizes contribute to the overall functionality and efficiency of the nanozymes in various catalytic applications. Interestingly, the 1:2:2 composite composed of $MnFe_2O_4$@Mn_3O_4|CuO showed a similar size to the $MnFe_2O_4$ nanozymes. This size similarity can be attributed to the role of $MnFe_2O_4$ as a nucleation site for the other Mn_3O_4 and CuO phases. During the synthesis process, $MnFe_2O_4$ particles likely provide a surface for the nucleation and growth of Mn_3O_4 and CuO, resulting in composite nanozymes with a size distribution influenced by the initial $MnFe_2O_4$ particles. This nucleation effect ensures a more uniform and controlled size of the composite, closely resembling the size of the pure $MnFe_2O_4$ nanozymes.

3.3. Electrochemical characterization of nanozymes

Fig. 4a shows the cyclic voltammogram of the magnetic nanostructures, $MnFe_2O_4$, observing two characteristic peaks corresponding to the irreversible Redox couple, Mn^{3+}/Mn^{4+}, around 0.634 and 0.244 V [35,36]. In contrast, the Mn_2O_3 nanostructure presents the same irreversible Redox couple but at more positive potentials, 0.860 and 0.416 V [37] (Fig. 4b). This shift can be associated with the non-presence of ferrite in the $MnFe_2O_4$ nanostructures, increasing the Redox couple's irreversibility by 0.055 V in Mn_3O_4. On the other hand, Fig. 4c shows the cyclic voltammogram of CuO nanostructures, where two Redox couples are observed, Cu^0/Cu^+ and Cu^+/Cu^{2+} at −0.034 and 0.169 V in the direction of the positive potentials, when reversing the direction of the sweep, they appear at −0.375 and −0.577 V, respectively [38,39]. Unlike the previous cyclic voltammograms, the potential range had to be reduced due to the higher catalytic activity presented by copper versus the hydrogen evolution reaction (HER). The current densities observed in the voltammograms are directly related to the available surface area of the nanostructure, which in turn correlates with the sizes observed in the TEM images for each of them (Fig. 3e).

Fig. 4d shows the cyclic voltammogram corresponding to the synthesized nanostructure at 1:2:2 ratios of $MnFe_2O_4$, Mn_3O_4, and CuO, respectively, where different peaks that were assigned to the presence of Cu and Mn are shown. Unlike the peaks observed in the CuO voltammogram, these appear to shift around 0.090 V towards more negative potential values, where the oxidation process of the copper species

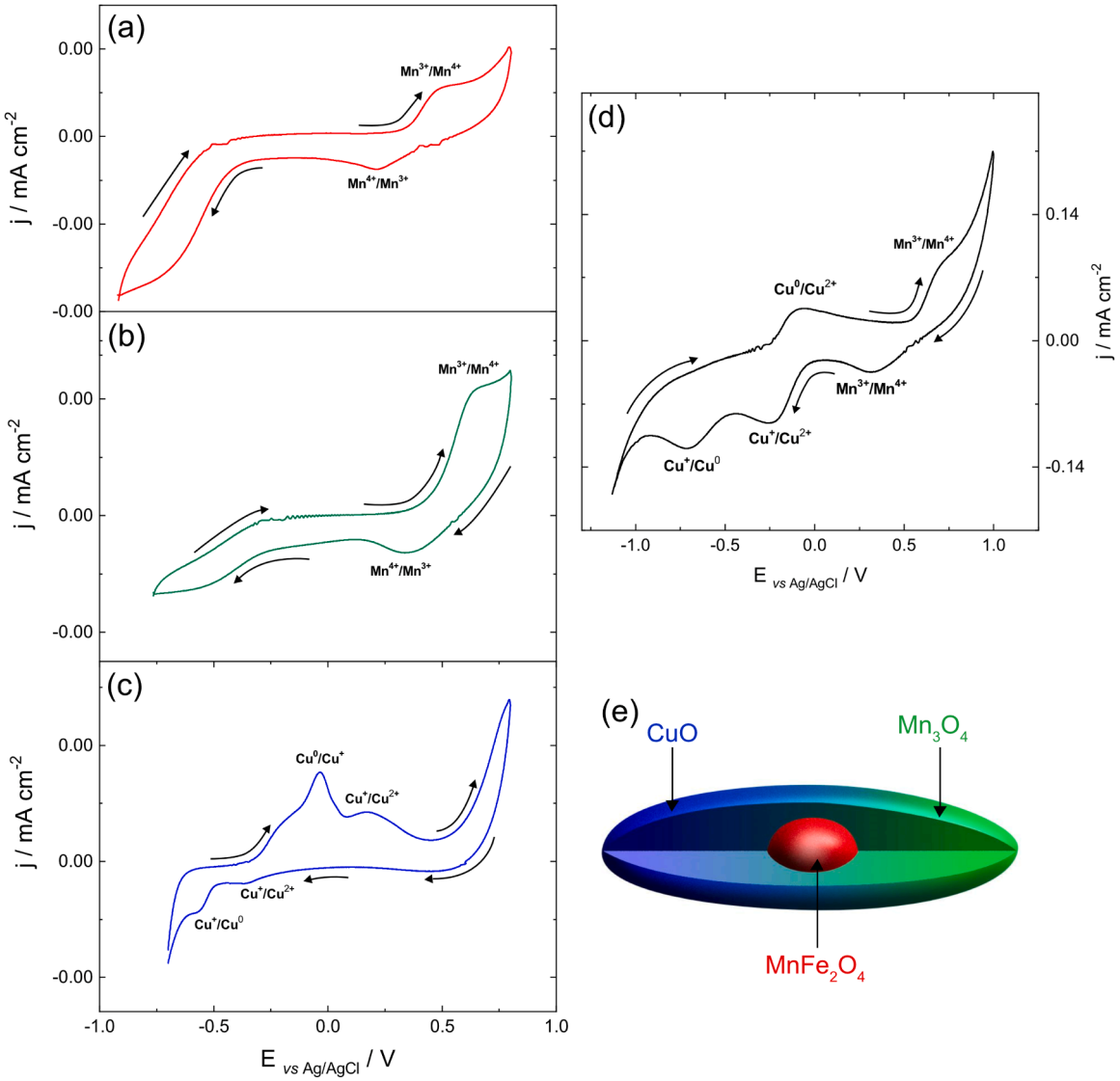

Fig. 4. Cyclic voltammetry of the nanostructures of: (a) $MnFe_2O_4$, (b) Mn_3O_4, (c) CuO and (d) $MnFe_2O_4$@CuO|Mn_3O_4 (1:2:2 nanozyme) in an acetate buffer solution pH 5 at $n = 0.05$ mVs^{-1}. (e) graphical representation of the nanostructure of $MnFe_3O_4$@CuO|Mn_3O_4.

shows a much wider signal around −0.059 V, overlapping two oxidation processes of Cu^0/Cu^+ and Cu^+/Cu^{2+}, whereas, when the potential sweep is reversed towards negative values, both well-defined reductions are shown with values of −0.259 and −0.716 V for Cu^{2+}/Cu^+ and Cu^+/Cu^0, respectively. Regarding the peaks observed at 0.749 and 0.319 V, they correspond to Redox couple Mn^{3+}/Mn^{4+} Redox couple, process irreversible with ΔE ca. 0.430 V, very similar to what was observed in the voltammogram corresponding to Mn_2O_3. From this, and as has been reported in the literature, it is possible to indicate what type of morphology or structure a material has from the voltammetric profiles [40,41]. In this instance, it is possible to determine that the nanostructure has a core@shell conformation, which contrasted with the TEM image, should be with a rice grain morphology (Fig. 3e)

3.4. Effect of redox mediators on catalytic activity of nanozymes

Redox mediators are primarily low molecular weight aromatic compounds that can be easily oxidized by natural laccase, converting them into highly active intermediates. These active mediators can then interact with and oxidize other compounds that are not susceptible to direct laccase oxidation. The active mediator transfers the electrons from the substrate to the enzyme, self-reducing in the process, thereby allowing the cycle to restart [42]. The use of redox mediators in laccase-like nanozyme-catalyzed processes has not yet been explored. Therefore, this study evaluated the effect of redox mediators to enhance the activity of the 1:2:2 nanozyme for expanding their potential use remediation of organic pollutants. Methyl orange was used as a model organic pollutant in this study due to its ease of spectrophotometric detection. It is a common azo dye widely used in the textile and dyeing industries, and its persistence in the environment makes it a representative compound for studying the degradation of organic pollutants [43]. It is estimated that over 70 % of industrial dyes are azo dyes. These compounds are characterized by the functional group (-N = N-), which links two identical or different alkyl or aryl radicals [44]. Three natural redox mediators (acetosyringone, syringaldehyde, and vanillin) and one synthetic redox mediator (1-Hydroxybenzotriazole) were included in the assays.

Fig. 5 shows the degradation efficiency of methyl orange using two concentrations of the 1:2:2 nanozyme (50 and 100 mg L^{-1}) in the absence and presence of redox mediators at different concentrations (25 μM, 50 μM, 75 μM, and 100 μM) and at pH 4 and 5. All treatments exhibited higher degradation rates at pH 4. In the absence of redox mediators, the 1:2:2 nanozyme achieved low degradation rates of methyl orange, with a maximum of 15.5 % using 100 mg L^{-1} nanozyme at pH 4. In absence of nanozymes, the redox mediators alone did not show any degradation of methyl orange. The addition of redox mediators to the system with nanozymes resulted in a substantial increase in the degradation of methyl orange. Acetosyringone was the most effective redox mediator, significantly enhancing the degradation of methyl orange, followed by syringaldehyde, vanillin, and 1-Hydroxybenzotriazole. No significant differences were observed at both nanozyme concentrations combined with acetosyringone, syringaldehyde, and HBT at pH 4, except for the treatment with 50 mg L^{-1} of nanozyme and 100 μM syringaldehyde. The treatment with acetosyringone demonstrated the highest efficiency, achieving near-complete degradation at concentrations of 50 μM and above. This resulted in a 6.3-fold increase compared to the no-mediator treatment at 100 mg L^{-1} nanozyme, indicating that acetosyringone is highly effective in facilitating the degradation process. Similar results were obtained with syringaldehyde; however, a noticeable decrease in the degradation of methyl orange was observed in the treatment with 100 μM of syringaldehyde and 50 mg L^{-1} of nanozyme. This phenomenon has also been observed in natural laccase-redox mediator systems, where high concentrations of redox mediators and low laccase levels can lead to the formation of non-productive complexes or enzyme inactivation [45]. Vanillin, while effective at pH 4, showed lower degradation efficiency compared to acetosyringone and syringaldehyde, with a maximum degradation of around 80 % at 100 μM, suggesting that higher concentrations are needed for optimal performance. Similarly, 1-Hydroxybenzotriazole exhibited moderate efficiency (60 %), with degradation rates improving as concentration increased at pH 4, although it reduced degradation at pH 5 compared to the no-mediator treatment. The observed effects of the different mediators can be attributed to their distinct pKa values, which influence their protonation states and subsequent reactivity. Both acetosyringone and syringaldehyde are syringyl-type phenolics with pKa values of 7.9 and 7.3 [46], indicating that at pH levels under pKa, the majority of their molecules are protonated. In contrast, the 1:2:2 nanozyme exhibits zeta potentials of −26.9 mV at pH 4 and −14.4 mV at pH 5. Therefore, the protonated forms of the mediators can easily interact with and be oxidized by the 1:2:2 nanozyme. Conversely, 1-Hydroxybenzotriazole has a pKa of 4.6 [47], which explains the higher degradation of methyl orange observed at pH 4 and the decreased degradation observed at pH 5. At pH slightly above 4.6, most 1-Hydroxybenzotriazole molecules are deprotonated, reducing their interaction with and oxidation by the 1:2:2 nanozyme. Vanillin is a guaiacyl-type phenolic has two pKa values: 7.4 for the hydroxyl (-OH) group [46] and 5.0 for the aldehyde group. This dual acidity leads to behavior similar to, but less pronounced than, that observed with 1-Hydroxybenzotriazole at pH 5. Specifically, at pH 5, the aldehyde group of vanillin is partially ionized, while the hydroxyl group remains mostly protonated. This partial ionization can influence the interaction and reactivity of vanillin in catalytic and oxidative processes. These results confirm the potential of redox mediators to enhance the application of nanozymes for pollutant degradation, mimicking the natural laccase-redox mediator system.

The degradation of methyl orange by natural laccase in presence and absence of redox mediators have been evaluated in several studies. Assays with laccase in absence of redox mediators have showed degradations between of 15 to 20 %, but in retention times between 5 and 6 h [48,49]. Laccase sole treatments showed rates degradation of methyl orange of 90 % after 30 h [14] and 68 % after 72 h [50]. While by using laccase mediator system with acetosyringone (200 mM) and syringaldehyde (200 mM) increase from 15 % to 80 % and 90 % degradation of methyl orange after 5 h, respectively [48]. Other approaches using immobilized laccase on chitosan-coated magnetic particles with 450 uM ABTS as redox mediators have reported methyl orange degradation rates of 60 % to 100 % after 1 h [43]. Another study using co-immobilized laccase and ABTS on PET/UiO-66(Zr)–NH_2 showed 21 % degradation of methyl orange with significant activity loss after 4 cycles [13]. Therefore, the efficiency natural laccase for degrading methyl orange is very limited. In recent studies on nanozymes, MnO_2/Cu-BDC—His laccase-like nanozymes achieved high degradation rates of nearly 80 % for methylene blue, alizarin red, neutral red, and aniline blue dyes within 30 min of reaction [51]. However, the degradation recalcitrance of these dyes, compared to methyl orange, can vary significantly. In this context, it has been reported that methyl orange exhibits greater degradation recalcitrance compared to methylene blue [52]. Peroxidase-like nanozymes have been evaluated to degrade methyl orange. Ag/Fe_3O_4@h-BN (75 mg L^{-1} catalyst) with 400 mM of H_2O_2 reached 99 % degradation of methyl orange in 40 min [53]. CeO_2@ZIF-8 (6 g L^{-1}) and 12 mM H_2O_2 showed 95.9 % in 5 h of treatment [54]. The use of natural redox mediators with laccase-like nanozymes, offers significant advantages over the use of H_2O_2 by peroxidase-like nanozymes. H_2O_2 can be toxic at high concentrations and lead to oxidative stress in biological systems, while natural redox mediators are generally less harmful. Their lower toxicity allows for safer applications in bioremediation and other environmental processes, making them more suitable for use in living organisms or sensitive ecosystems [55]. Fig. 6a presents the concentration of MO relative to its initial concentration (C/C_0) over time. It can be observed that the presence of acetosyringone (1:2:2/AS), MO degrades significantly faster, with its concentration rapidly decreasing and nearly reaching complete degradation within 800 s. This rapid decrease highlights the enhanced catalytic activity provided by the

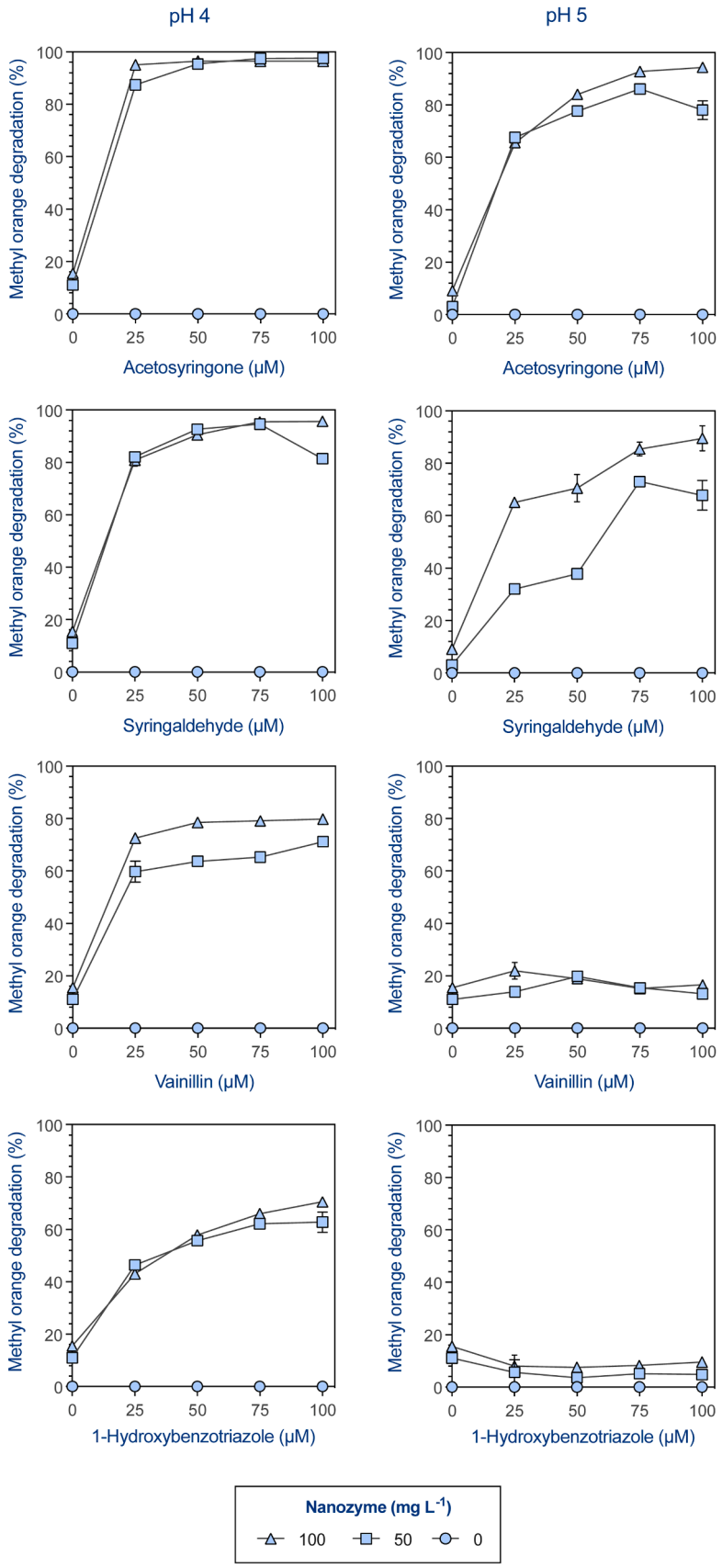

Fig. 5. Effect of natural redox mediators (acetosyringone, syringaldehyde, and vanillin) and 1-hydroxybenzotriazole concentration on the degradation of MO by 1:2:2 nanozyme at pH 4 and 5 after 15 min. The data presented represent the mean values with standard deviations ($n = 3$).

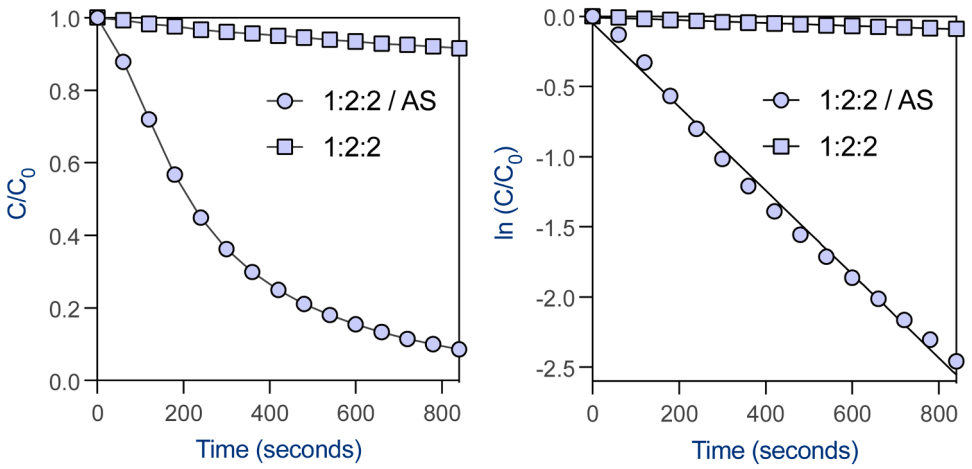

Fig. 6. Kinetics of MO degradation by Nanozyme with and without acetosyringone acting as the redox mediator (k = 0.192 min^{-1} and k = 0,00,618 min^{-1}).

redox mediator, which facilitates the degradation of MO by the nanocomposite. In contrast, in the absence of acetosyringone (1:2:2), the degradation of MO is markedly slower, with only a slight reduction in MO concentration over the same period. This stark difference in degradation rates underscores the critical role of the redox mediator in accelerating the catalytic reaction. The presence of acetosyringone significantly boosts the efficiency of the 1:2:2 nanozyme, enabling more effective degradation of MO. Fig. 6b shows the data fitted to a first-order kinetic model. The rate constants for the degradation reactions are k = 0.192 min^{-1} with acetosyringone and k = 0.00618 min^{-1} without the mediator. These results highlight the potential of combining nanocomposites with suitable redox mediators to achieve effective environmental remediation, significantly improving the degradation rates of harmful compounds.

3.5. Cyclic voltammetry of redox mediators and 1:2:2 nanozyme

Fig. 7a shows the cyclic voltammogram corresponding to the oxidation of acetosyringone, where three characteristic peaks appear, one at 0.397 V associated with the oxidation of acetosyringone (Scheme 1a) and at 0.616 and 0.841 V corresponding to the polymerisation process described in the literature [56]. When the nanozyme is added, the voltammetric profile is modified in the two processes described, where the polymerisation processes increase their charge by 23 and 72 % respectively. In contrast, the peak corresponding to the oxidation of acetosyringone disappears completely, indicating that the catalytic process of enolate ion formation is generated by $MnFe_3O_4$@CuO|Mn_3O_4 (Scheme 1b), very different from that described for the catalysis of acetosyringone in the presence of laccase enzyme, which occurs via two complementary routes, Electron transfer (ET) route and radical hydrogen atom transfer (HAT) and shows a 50 % decrease in the peak current of the oxidation process [57], indicating that the 1:2:2 nanozyme has higher catalytic power than natural laccase. Fig. 7b shows the cyclic voltammogram corresponding to the oxidation of syringaldehyde, where two characteristic peaks are observed without the nanozyme at 0.793 and 0.615 V corresponding to the oxidation of syringaldehyde to syringic acid and syringic acid to 2,6-dimethoxy-1,4-benzoquinone, respectively. Furthermore, two much weaker signals at 0.548 and 0.191 V correspond to the reduction processes [58,59]. In the presence of nanozyme, the quenching of the signals corresponding to syringaldehyde oxidation is immediately observed, and only the reduction processes at 0.603 and 0.048 V are observed. The reaction steps that have been described in the literature for the presence of laccase [60] serve as a platform to demonstrate that the presence of nanozyme plays the same role as the enzyme in the oxidation of syringaldehyde; this can be attributed to the catalytic properties of $MnFe_2O_4$ [61], which are exacerbated in the presence of CuO and Mn_3O_4 as described in the literature [62,63] (Scheme 2).

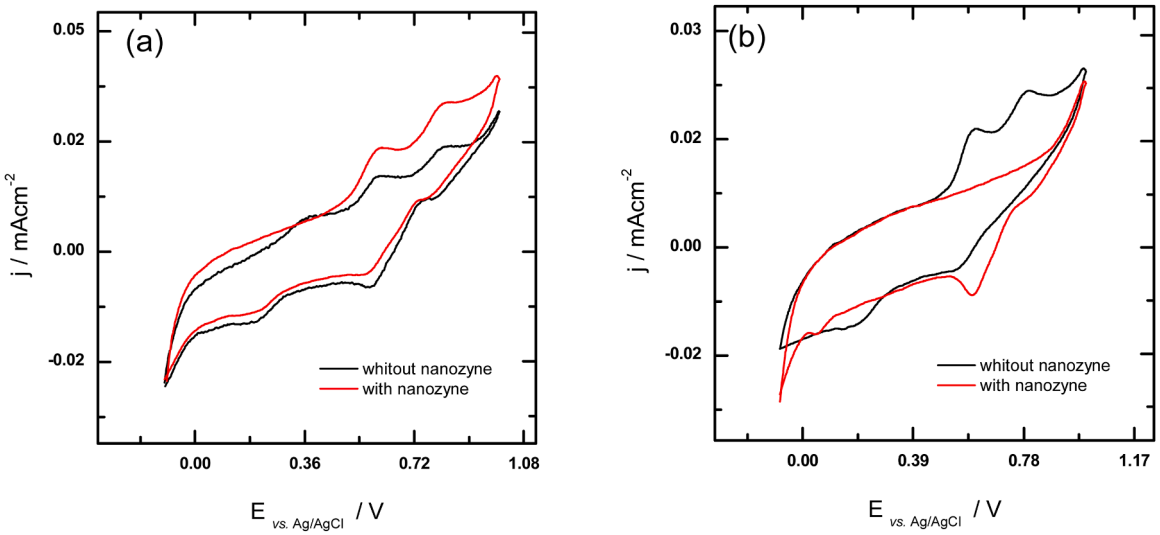

Fig. 7. Cyclic Voltammogram of (a) acetosyringone with and without nanozyme and (b) syringaldehyde whit and without nanozyme, a scan rate of 0.050 V s^{-1}.

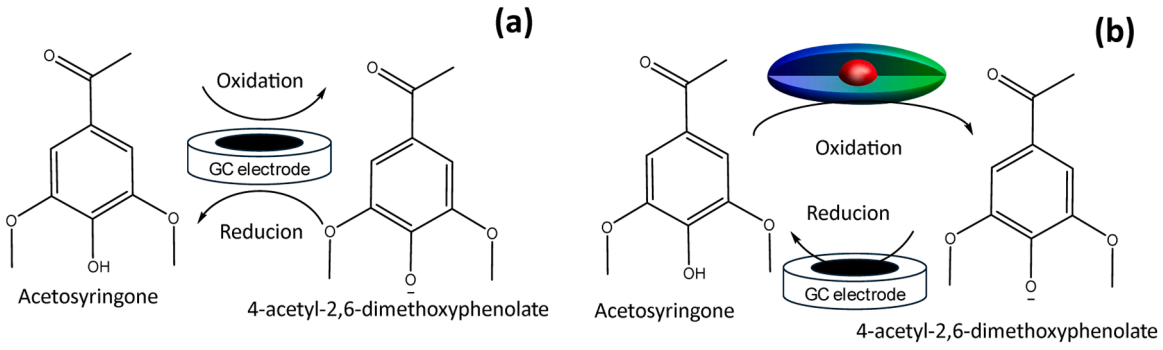

Scheme 1. Diagram of the oxidation and reduction process of acetosyringone (a) without nanozyme and (b) with nanozyme.

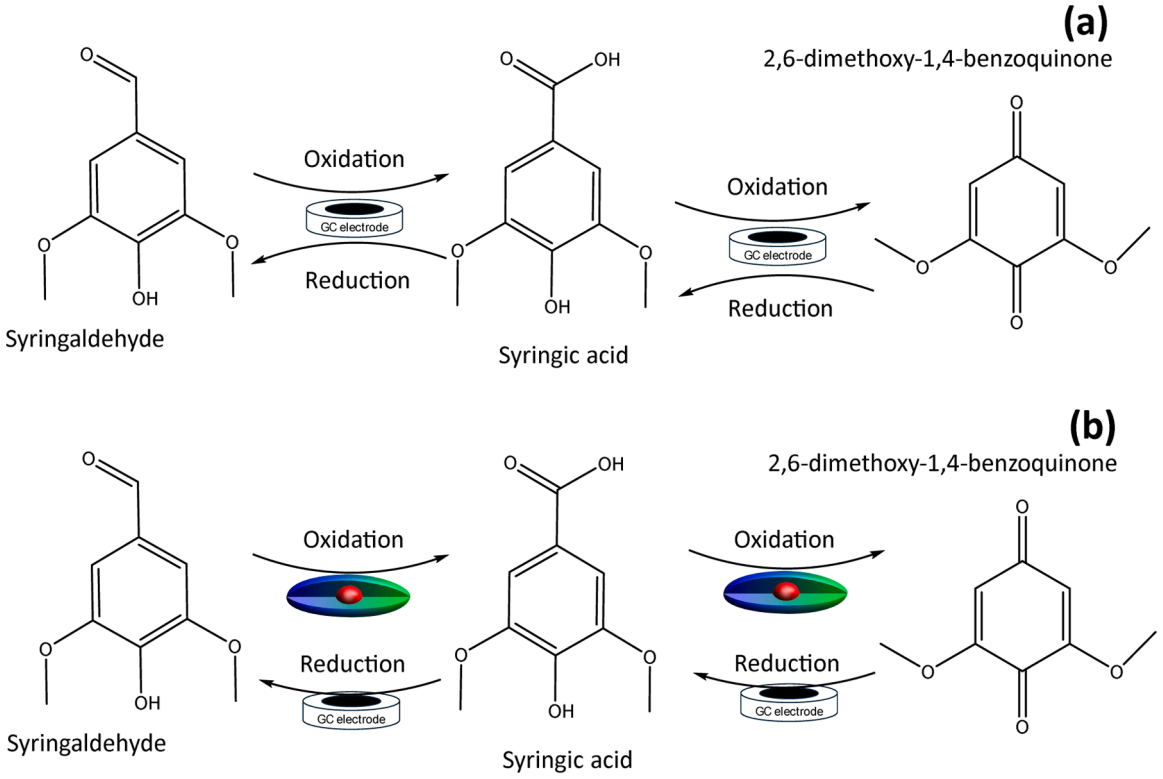

Scheme 2. Diagram of the oxidation and reduction process of Syringaldehyde (a) without nanozyme and (b) with nanozyme.

Thus, it is possible to propose that the presence of the CuO and Mn_3O_4 alloy coating the metallic centre of $MnFe_2O_4$, forming a core@shell with a rice-grain morphology, has a catalytic activity superior to that presented by the natural Laccase enzyme [64].

3.6. *Reuse and stability of nanozymes for methyl orange degradation*

The recovery and reusability of nanozymes were evaluated following the degradation of methyl orange. Recovery was achieved by using an external magnet to attract the nanozymes (Fig. 8a). After separating the supernatant, the nanozyme pellet was washed three times with water and reused in subsequent degradation cycles. The nanozymes demonstrated effective reusability for up to five cycles, achieving a maximum degradation efficiency of 87 % (Fig. 8b). However, their efficiency declined in the sixth and seventh cycles, with degradation to 67 % and 32 %, respectively. Similarly, Xu et al. (2021) reported a significant loss of activity in laccase-like nanozymes based on the coordination of copper with a cysteine–aspartic acid (Cys–Asp) dipeptide after four cycles [65]. Metal leaching was assessed after each cycle, revealing a cumulative release of Mn and Cu ions (Fig. 7b). To determine whether these ions contributed to catalysis, their potential activity in methyl orange degradation was evaluated, both in the presence and absence of redox mediators. The results confirmed that these ions exhibited no catalytic activity. Furthermore, studies have shown that Cu^{2+} ions at concentrations as low as 1.2 mg L^{-1} can inhibit the laccase-like activity of Mn_3O_4 nanozymes [23]. This suggests that the observed decline in degradation efficiency is primarily due to the loss of structural integrity in the nanozymes. Although the 1:2:2 nanozymes have demonstrated remarkable efficiency in the degradation of methyl orange and perform particularly well when paired with redox mediators. Their application could present environmental risks and challenges related to metal leaching. The release of metal ions poses significant toxicity risks, as some ions have been related to adverse human health effects [66,67]. From an ecological perspective, the leaching of metals into ecosystems raises concerns about environmental toxicity and bioaccumulation. For instance, studies have shown that certain metal-based nanoparticles can inhibit algal growth, highlighting potential ecological impacts [68]. Additionally, the challenges associated with efficiently recovering

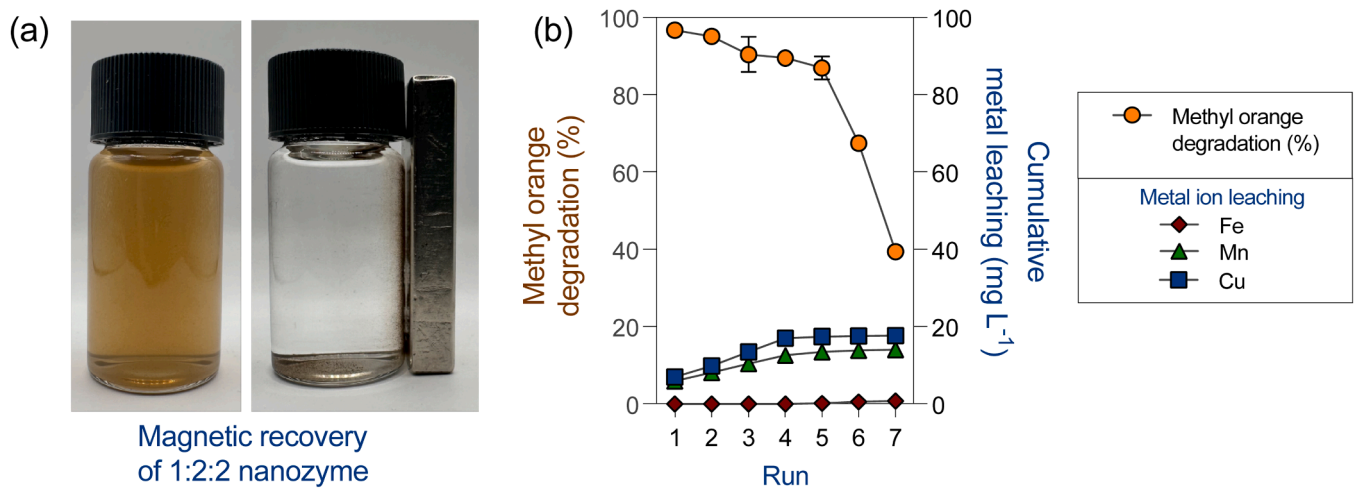

Fig. 8. (a) Images showing the magnetic recovery of the 1:2:2 nanozyme, (b) its reuse in consecutive cycles of methyl orange degradation, and (c) the cumulative metal ion leaching after each cycle. The data represent mean values with standard deviations ($n = 3$).

nanozymes after use may amplify the risk of environmental contamination. Addressing these issues is essential for enabling the safe and sustainable application of nanozymes in environmental remediation [66,68]. To mitigate metal leaching and improve nanozyme stability, several strategies have been proposed. These include the use of support materials such as carbon, SiO_2, and Al_2O_3 [69,70], as well as the covalent modification of metal oxide surfaces with silane, phosphonate, amines, and other stabilizing agents [71].

4. Conclusion

This study on the laccase-like activity of multimetallic nanozymes provides significant insights into their catalytic performance and the synergistic effects of various metal oxides ($MnFe_2O_4$, Mn_3O_4, and CuO). The incorporation of a $MnFe_2O_4$ core not only endowed the nanozymes with laccase-like activity but also imparted magnetic properties facilitating their recovery by using an external magnetic field. Our findings demonstrate that redox mediators substantially enhance the degradation efficiency of methyl orange, highlighting the potential application of these nanozymes in environmental remediation. Among the mediators tested, acetosyringone (a syringyl-type phenolic) proved to be the most effective, achieving near-complete degradation at concentrations of 50 μM and above, resulting in a 6.3-fold increase compared to treatments without mediators. The observed synergistic effects and increased activity with redox mediators underscore the promising potential of nanozymes for environmental applications. Future research should prioritize integrating this nanozyme into support materials that prevent metal leaching, ensuring a safe process, and further assess its performance with a wider variety of pollutants, including more complex and real-world contaminants.

CRediT authorship contribution statement

E. Hermosilla: Writing – review & editing, Writing – original draft, Methodology, Investigation, Funding acquisition, Data curation, Conceptualization. **M. Diaz:** Methodology, Data curation, Conceptualization. **M.J. Pérez-Vélez:** Methodology, Data curation, Conceptualization. **S. Leiva:** Conceptualization, Data curation, Methodology. **A.M.R. Ramírez:** Writing – review & editing, Writing – original draft, Methodology, Data curation, Conceptualization. **M.R.V. Lanza:** Writing – review & editing, Formal analysis. **O. Rubilar:** Writing – review & editing, Methodology, Formal analysis.

Declaration of competing interest

The authors declare the following financial interests/personal relationships which may be considered as potential competing interests:

Edward Hermosilla reports financial support was provided by National Fund For Scientific Technological and Technological Innovation Development. Andres Ramirez reports financial support was provided by National Fund For Scientific Technological and Technological Innovation Development. Olga Rubilar reports financial support was provided by National Commission for Scientific and Technological Research Funds for Research Centers in Priority Areas. If there are other authors, they declare that they have no known competing financial interests or personal relationships that could have appeared to influence the work reported in this paper.

Acknowledgements

This work was financed by ANID/FONDECYT Iniciación 11230939 and ANID/FONDAP 1523A0001 and ANID/FONDECYT 1230426 projects. We also thank the Scientific and Technological Bioresource Nucleus of Universidad de La Frontera (BIOREN–UFRO) and project Service Management Analytical Research and Training Center (SmartC-BIOREN) N °CCSS210005.

Data availability

No data was used for the research described in the article.

References

[1] L. Arregui, M. Ayala, X. Gómez-Gil, G. Gutiérrez-Soto, C.E. Hernández-Luna, M. Herrera De Los Santos, L. Levin, A. Rojo-Domínguez, D. Romero-Martínez, M.C. N. Saparrat, M.A. Trujillo-Roldán, N.A. Valdez-Cruz, Laccases: structure, function, and potential application in water bioremediation, Microb. Cell Fact. 18 (2019), https://doi.org/10.1186/s12934-019-1248-0.

[2] C.A. Gasser, E.M. Ammann, P. Shahgaldian, P.F.X. Corvini, Laccases to take on the challenge of emerging organic contaminants in wastewater, Appl. Microbiol. Biotechnol. 98 (2014), https://doi.org/10.1007/s00253-014-6177-6.

[3] M. Bilal, M. Asgher, R. Parra-Saldivar, H. Hu, W. Wang, X. Zhang, H.M.N. Iqbal, Immobilized ligninolytic enzymes: an innovative and environmental responsive technology to tackle dye-based industrial pollutants – a review, Sci. Total Environ. 576 (2017), https://doi.org/10.1016/j.scitotenv.2016.10.137.

[4] H. Cabana, J.L.H. Jiwan, R. Rozenberg, V. Elisashvili, M. Penninckx, S.N. Agathos, J.P. Jones, Elimination of endocrine disrupting chemicals nonylphenol and bisphenol A and personal care product ingredient triclosan using enzyme preparation from the white rot fungus coriolopsis polyzona, Chemosphere 67 (2007), https://doi.org/10.1016/j.chemosphere.2006.10.037.

[5] H. Chakroun, T. Mechichi, M.J. Martinez, A. Dhouib, S. Sayadi, Purification and characterization of a novel laccase from the ascomycete trichoderma atroviride:

application on bioremediation of phenolic compounds, Process Biochem. 45 (2010), https://doi.org/10.1016/j.procbio.2009.11.009.
[6] X. Xu, J. Wang, R. Huang, W. Qi, R. Su, Z. He, Preparation of laccase mimicking nanozymes and their catalytic oxidation of phenolic pollutants, Catal. Sci. Technol. 11 (2021) 3402–3410, https://doi.org/10.1039/d1cy00074h.
[7] K. González Arzola, Y. Gimeno, M.C. Arévalo, M.A. Falcón, A. Hernández Creus, Electrochemical and AFM characterization on gold and carbon electrodes of a high redox potential laccase from Fusarium proliferatum, Bioelectrochemistry 79 (2010), https://doi.org/10.1016/j.bioelechem.2009.10.001.
[8] I. Mateljak, E. Monza, M.F. Lucas, V. Guallar, O. Aleksejeva, R. Ludwig, D. Leech, S. Shleev, M. Alcalde, Increasing redox potential, redox mediator activity, and stability in a fungal laccase by computer-guided mutagenesis and directed evolution, ACS Catal. 9 (2019), https://doi.org/10.1021/acscatal.9b00531.
[9] C. Liers, E. Aranda, E. Strittmatter, K. Piontek, D.A. Plattner, H. Zorn, R. Ullrich, M. Hofrichter, Phenol oxidation by DyP-type peroxidases in comparison to fungal and plant peroxidases, J. Mol. Catal. B Enzym. 103 (2014), https://doi.org/10.1016/j.molcatb.2013.09.025.
[10] Y. Xu, Y. Anker, M.P. Talawar, Degradation of tetracycline, oxytetracycline & ampicillin by purified multiple copper oxidase like laccase from Stentrophomonas sp. YBX1, Braz. J. Microbiol. (2024), https://doi.org/10.1007/s42770-024-01247-8.
[11] J. Benali, I. Ben Atitallah, B. Ghariani, T. Mechichi, B. Hadrich, H. Zouari-Mechichi, Optimized decolorization of two poly azo dyes Sirius Red and Sirius Blue using laccase-mediator system, 3 Biotech 14 (2024). 10.1007/s13205-024-03937-4.
[12] C. Zhang, S. You, J. Zhang, W. Qi, R. Su, Z. He, An effective in-situ method for laccase immobilization: excellent activity, effective antibiotic removal rate and low potential ecological risk for degradation products, Bioresour. Technol. 308 (2020), https://doi.org/10.1016/j.biortech.2020.123271.
[13] X. Lou, F. Zhi, X. Sun, F. Wang, X. Hou, C. Lv, Q. Hu, Construction of co-immobilized laccase and mediator based on MOFs membrane for enhancing organic pollutants removal, Chem. Eng. J. 451 (2023), https://doi.org/10.1016/j.cej.2022.138080.
[14] X.S. Tan, S.J. Wang, K.Y. Wu, P. Qi, P.W. Hu, J. Zhang, Optimization of conditions for laccase production by Pleurotus eryngii and application of laccase to azo dye methyl orange decolorization, Mycosystema 38 (2019), https://doi.org/10.13346/j.mycosystema.190167.
[15] H.Y. Kim, J.K. Ahn, M. il Kim, K.S. Park, H.G. Park, Rapid and label-free, electrochemical DNA detection utilizing the oxidase-mimicking activity of cerium oxide nanoparticles, Electrochem. Commun. (2019), https://doi.org/10.1016/j.elecom.2018.12.008.
[16] H. Deng, S. He, X. Lin, L. Yang, Z. Lin, R. Chen, H. Peng, W. Chen, Target-triggered inhibiting oxidase-mimicking activity of platinum nanoparticles for ultrasensitive colorimetric detection of silver ion, Chin. Chem. Lett. (2019), https://doi.org/10.1016/j.cclet.2019.05.032.
[17] X. Niu, K. Ye, Z. Li, H. Zhao, L. Wang, J. Pan, H. Song, M. Lan, Pyrophosphate-mediated on–Off–On oxidase-like activity switching of nanosized MnFe2O4 for alkaline phosphatase sensing, J. Anal. Test. (2019), https://doi.org/10.1007/s41664-019-00100-4.
[18] L. Guo, L. Mao, K. Huang, H. Liu, Pt–Se nanostructures with oxidase-like activity and their application in a selective colorimetric assay for mercury(II), J. Mater. Sci. (2017), https://doi.org/10.1007/s10853-017-1181-8.
[19] W. Lu, J. Shu, Z. Wang, N. Huang, W. Song, The intrinsic oxidase-like activity of Ag2O nanoparticles and its application for colorimetric detection of sulfite, Mater. Lett. (2015), https://doi.org/10.1016/j.matlet.2015.04.051.
[20] C. Li, Y. Sun, X. Li, S. Fan, Y. Liu, X. Jiang, M.D. Boudreau, Y. Pan, X. Tian, J.J. Yin, Bactericidal effects and accelerated wound healing using Tb 4 O 7 nanoparticles with intrinsic oxidase-like activity, J. Nanobiotechnol. (2019), https://doi.org/10.1186/s12951-019-0487-x.
[21] A.A. Vernekar, T. Das, S. Ghosh, G. Mugesh, A remarkably efficient MnFe2O4-based oxidase nanozyme, Chem. Asian J. 11 (2016) 72–76, https://doi.org/10.1002/asia.201500942.
[22] E. Hermosilla, A.B. Seabra, I.M. Lourenço, F.F. Ferreira, G. Tortella, O. Rubilar, Highly sensitive oxidation of MBTH/DMAB by MnFe2O4 nanoparticles as a promising method for nanozyme-based sensor development, Colloids Surf. A Physicochem. Eng. Asp. 621 (2021), https://doi.org/10.1016/j.colsurfa.2021.126585.
[23] Z. Wu, Y. Wei, Y. Tang, L. Xia, X. Niu, Y. Wu, Switching off-on colorimetric sensor for rapid and selective detection of histamine in aquatic products based on Cu2+-mediated laccase-mimic activity of Mn3O4 nanoparticles, Food Control 170 (2025) 111056, https://doi.org/10.1016/J.FOODCONT.2024.111056.
[24] R. Zhang, X. Yan, K. Fan, Nanozymes inspired by natural enzymes, Acc. Mater. Res. 2 (2021) 534–547, https://doi.org/10.1021/ACCOUNTSMR.1C00074/ASSET/IMAGES/MEDIUM/MR1C00074_0007.GIF.
[25] S. Bhagat, J. Shah, S. Singh, Metal-based nanozyme: strategies to modulate the catalytic activity to realize environment application, in: H.K. Daima, N. PN, E. Lichtfouse (Eds.), Nanozymes For Environmental Engineering, Springer International Publishing, Cham, 2021: pp. 177–212. 10.1007/978-3-030-68230-9_7.
[26] A. Rezagholizade-shirvan, A. Ghasemi, Y. Mazaheri, S. Shokri, S. Fallahizadeh, M. Alizadeh Sani, M. Mohtashami, M. Mahmoudzadeh, M. Sarafraz, M. Darroudi, Z. Rezaei, E. Shamloo, Removal of aflatoxin M1 in milk using magnetic laccase/MoS2/chitosan nanocomposite as an efficient sorbent, Chemosphere 365 (2024) 143334, https://doi.org/10.1016/J.CHEMOSPHERE.2024.143334.
[27] J. Sánchez-Ramírez, J.L. Martínez-Hernández, R.G. López-Campos, E.P. Segura-Ceniceros, H. Saade, R. Ramos-González, M.G. Neira-Velázquez, M.A. Medina-Morales, C.N. Aguilar, A. Ilyina, Laccase validation as pretreatment of agave waste prior to saccharification: free and immobilized in superparamagnetic nanoparticles enzyme preparations, Waste BioMass Valorization 9 (2018) 223–234, https://doi.org/10.1007/s12649-016-9774-z.
[28] S. Huang, X. Tang, L. Yu, S. Hong, J. Liu, B. Xu, R. Liu, Y. Guo, L. Xu, Colorimetric assay of phosphate using a multicopper laccase-like nanozyme, Microchim. Acta 189 (2022), https://doi.org/10.1007/s00604-022-05476-2.
[29] F. Xiao, Q. Xia, S. Zhang, Q. Li, D. Chen, H. Li, D. Yang, Y. Yang, Ultrasound and defect engineering-enhanced nanozyme with high laccase-like activity for oxidation and detection of phenolic compounds and adrenaline, J. Hazard. Mater. 465 (2024), https://doi.org/10.1016/j.jhazmat.2023.133126.
[30] L. Yang, X.Y. Guo, Q.H. Zheng, Y. Zhang, L. Yao, Q.X. Xu, J.C. Chen, S. Bin He, W. Chen, Construction of platinum nanozyme by using carboxymethylcellulose with improved laccase-like activity for phenolic compounds detection, Sens. Actuators. B Chem. 393 (2023), https://doi.org/10.1016/j.snb.2023.134165.
[31] X. Liu, F. Wang, C. Xia, Q. You, X. Chen, Y. Li, W. Lin, L. Guo, F. Fu, Copper nanoparticles incorporated nitrogen-rich carbon nitride as laccase-like nanozyme for colorimetric detection of bisphenol a released from microplastics, Microchem. J. 190 (2023), https://doi.org/10.1016/j.microc.2023.108682.
[32] S. Shirsat, D. Pawar, N.J.J. Pawar, V.S. Tale, R. Henry, Synthesis of copper oxide nanoparticles by chemical precipitation method for the determination of antibacterial efficacy against Streptococcus sp. and Staphylococcus sp, Asian J. Pharm. Clin. Res. (2019), https://doi.org/10.22159/ajpcr.2019.v12i5.32270.
[33] A. Zerva, C. Pentari, A. Termentzi, A.H.P. America, D. Zouraris, S.K. Bhattacharya, A. Karantonis, G.I. Zervakis, E. Topakas, Discovery of two novel laccase-like multicopper oxidases from Pleurotus citrinopileatus and their application in phenolic oligomer synthesis, Biotechnol. Biofuels 14 (2021), https://doi.org/10.1186/s13068-021-01937-7.
[34] L. Gao, J. Zhuang, L. Nie, J. Zhang, Y. Zhang, N. Gu, T. Wang, J. Feng, D. Yang, S. Perrett, X. Yan, Intrinsic peroxidase-like activity of ferromagnetic nanoparticles, Nat. Nanotechnol. (2007), https://doi.org/10.1038/nnano.2007.260.
[35] S. Kogularasu, M. Akilarasan, S.M. Chen, E. Elaiyappillai, P.M. Johnson, T. W. Chen, F.M.A. Al-Hemaid, M.A. Ali, M.S. Elshikh, A comparative study on conventionally prepared MnFe2O4 nanospheres and template-synthesized novel MnFe2O4 nano-agglomerates as the electrodes for biosensing of mercury contaminations and supercapacitor applications, Electrochim. Acta 290 (2018), https://doi.org/10.1016/j.electacta.2018.09.028.
[36] A. Sivakumar, S. Sahaya Jude Dhas, P. Sivaprakash, A.I. Almansour, R. Suresh Kumar, N. Arumugam, K. Perumal, S. Arumugam, S.A. Martin Britto Dhas, Raman spectroscopic and electrochemical measurements of dynamic shocked MnFe2O4 nano-crystalline materials, J. Inorg. Organomet. Polym. Mater. 32 (2022), https://doi.org/10.1007/s10904-021-02111-0.
[37] H. Wang, T. Wang, G. Stevenson, M. Chamoun, R.W. Lindström, MnO2/Mn2+ chemistry: charging protocol and electrolyte regulation, Energy Storage Mater. 63 (2023), https://doi.org/10.1016/j.ensm.2023.103008.
[38] E.M.S. Elfeky, M.R. Shehata, Y.H. Elbashar, M.H. Barakat, W.M.A. El Rouby, Developing the sensing features of copper electrodes as an environmental friendly detection tool for chemical oxygen demand, RSC Adv. 12 (2022), https://doi.org/10.1039/d1ra09411d.
[39] S. Mohammadzadeh, H.R. Zare, H. Khoshro, Electrochemical study of Cu2O/CuO composite coating produced by annealing and electrochemical methods, J. Iran. Chem. Soc. 16 (2019), https://doi.org/10.1007/s13738-019-01736-w.
[40] J. Lorca-Ponce, E. Urzúa, F. Ávila-Salas, A.M. Ramírez, M. Ahumada, Silver nanoparticle's size and morphology relationship with their electrocatalysis and detection properties, Appl. Surf. Sci. 617 (2023), https://doi.org/10.1016/j.apsusc.2023.156584.
[41] E. Urzúa, F. Gonzalez-Torres, V. Beltrán, P. Barrias, S. Bonardd, A.M.R. Ramírez, M. Ahumada, Ag@Au bimetallic nanoparticles: an easy and highly reproducible synthetic approach for photocatalysis, Nanoscale Adv. 4 (2022), https://doi.org/10.1039/d2na00539e.
[42] I. Bassanini, E.E. Ferrandi, S. Riva, D. Monti, Biocatalysis with laccases: an updated overview, Catalysts 11 (2020) 26, https://doi.org/10.3390/CATAL11010026, 2021Page 26 11.
[43] T.R. Silveira, C.D. Ebling, L.D. Magro, R.C. Rodrigues, W.D. Hahn Schneider, M. Camassola, E. Weber de Menezes, Á. Meneguzzi, M.P. Klein, An efficient decolorization of methyl orange dye by laccase from Marasmiellus palmivorus immobilized on chitosan-coated magnetic particles, Biocatal. Agric. Biotechnol. 30 (2020), https://doi.org/10.1016/j.bcab.2020.101859.
[44] S. Benkhaya, S. M'rabet, A. El Harfi, Classifications, properties, recent synthesis and applications of azo dyes, Heliyon 6 (2020), https://doi.org/10.1016/J.HELIYON.2020.E03271.
[45] A. Kunamneni, F. Plou, A. Ballesteros, M. Alcalde, Laccases and their applications: a patent review, Recent Pat. Biotechnol. 2 (2008), https://doi.org/10.2174/187220808783330965.
[46] D. Silva, A.C. Sousa, M.P. Robalo, L.O. Martins, A wide array of lignin-related phenolics are oxidized by an evolved bacterial dye-decolourising peroxidase, New Biotechnol. 77 (2023), https://doi.org/10.1016/j.nbt.2022.12.003.
[47] R. Chen, L. Guo, S. Xu, Experimental and theoretical investigation of 1-hydroxy-benzotriazole as a corrosion inhibitor for mild steel in sulfuric acid medium, Int. J. Electrochem. Sci. 9 (2014), https://doi.org/10.1016/s1452-3981(23)10938-2.
[48] I. Pardo, X. Chanagá, A.I. Vicente, M. Alcalde, S. Camarero, New colorimetric screening assays for the directed evolution of fungal laccases to improve the conversion of plant biomass, BMC Biotechnol. 13 (2013), https://doi.org/10.1186/1472-6750-13-90.

[49] T. Bu, R. Yang, Y.J. Zhang, Y. Cai, Z. Tang, C. Li, Q. Wu, H. Chen, Improving decolorization of dyes by laccase from Bacillus licheniformis by random and site-directed mutagenesis, PeerJ 8 (2020), https://doi.org/10.7717/peerj.10267.
[50] A.S. Abd El-latif, A.N.A. Zohri, H.M. El-Aref, G.A.E. Mahmoud, Kinetic studies on optimized extracellular laccase from Trichoderma harzianum PP389612 and its capabilities for azo dye removal, Microb. Cell Fact. 23 (2024) 150, https://doi.org/10.1186/s12934-024-02412-2.
[51] M. Li, Y. Xie, X. Su, Versatile laccase-mimicking enzyme for dye decolorization and tetracyclines identification upon a colorimetric array sensor, J. Hazard. Mater. 483 (2025) 136683, https://doi.org/10.1016/J.JHAZMAT.2024.136683.
[52] C.H. Nguyen, C.C. Fu, R.S. Juang, Degradation of methylene blue and methyl orange by palladium-doped TiO2 photocatalysis for water reuse: efficiency and degradation pathways, J. Clean. Prod. (2018) 202, https://doi.org/10.1016/j.jclepro.2018.08.110.
[53] Z. Xin, K. Duan, Q. Zhuo, Q. He, X. Zhang, C. Zheng, X. Han, T. Han, Z. Fu, X. Xu, X. Zhao, Novel nanozyme Ag/Fe3O4@h-BN with peroxidase-mimicking and oxidase-mimicking activities for dye degradation, As(V) removal and detection, Chem. Eng. J. 461 (2023), https://doi.org/10.1016/j.cej.2023.141589.
[54] T. Yang, X. Liu, Z. Zeng, X. Wang, P. Zhang, B. Feng, K. Tian, T. Qing, Efficient and recyclable degradation of organic dye pollutants by CeO2@ZIF-8 nanozyme-based non-photocatalytic system, Environ. Pollut. 316 (2023), https://doi.org/10.1016/j.envpol.2022.120643.
[55] P. Mani, V.T.F. Kumar, T. Keshavarz, T. Sainathan Chandra, G. Kyazze, The role of natural laccase redox mediators in simultaneous dye decolorization and power production in microbial fuel cells, Energies (2018) 11, https://doi.org/10.3390/en11123455 (Basel).
[56] C. Fernández-Sánchez, T. Tzanov, G.M. Gübitz, A. Cavaco-Paulo, Voltammetric monitoring of laccase-catalysed mediated reactions, Bioelectrochemistry 58 (2002), https://doi.org/10.1016/S1567-5394(02)00119-6.
[57] Y. Du, H. Ma, L. Huang, Y. Pan, J. Huang, Y. Liu, Electrochemical characteristics of the decolorization of three dyes by laccase mediator system (LMS) with synthetic and natural mediators, Chemosphere 239 (2020), https://doi.org/10.1016/j.chemosphere.2019.124779.
[58] N. Volkova, V. Ibrahim, R. Hatti-Kaul, Laccase catalysed oxidation of syringic acid: calorimetric determination of kinetic parameters, Enzyme Microb. Technol. 50 (2012), https://doi.org/10.1016/j.enzmictec.2012.01.005.
[59] H. Lin, J. Su, Y. Liu, L. Yang, Catalytic conversion of lignocellulosic biomass to value-added organic acids in aqueous Media, in: 2014. 10.1007/978-3-642-54458-3_5.
[60] L. Maarit, K. Kristiina, H. Petri, S. Jussi, On the reactions of two fungal laceases differing in their redox potential with lignin model compounds: products and their rate of formation, J. Agric. Food Chem. 57 (2009), https://doi.org/10.1021/jf901511k.
[61] X. Zhou, L. Kong, Z. Jing, S. Wang, Y. Lai, M. Xie, L. Ma, Z. Feng, J. Zhan, Facile synthesis of superparamagnetic β-CD-MnFe2O4 as a peroxymonosulfate activator for efficient removal of 2,4- dichlorophenol: structure, performance, and mechanism, J. Hazard. Mater. 394 (2020), https://doi.org/10.1016/j.jhazmat.2020.122528.
[62] J.C. Villar, A. Caperos, F. García-Ochoa, Oxidation of hardwood kraft-lignin to phenolic derivatives with oxygen as oxidant, Wood Sci. Technol. 35 (2001), https://doi.org/10.1007/s002260100089.
[63] R. Abejón, H. Pérez-Acebo, L. Clavijo, Alternatives for chemical and biochemical lignin valorization: hot topics from a bibliometric analysis of the research published during the 2000-2016 period, Processes 6 (2018), https://doi.org/10.3390/pr6080098.
[64] Z. Gao, Y. Yi, J. Zhao, Y. Xia, M. Jiang, F. Cao, H. Zhou, P. Wei, H. Jia, X. Yong, Co-immobilization of laccase and TEMPO onto amino-functionalized magnetic Fe3O4 nanoparticles and its application in acid fuchsin decolorization, Bioresour. Bioprocess. 5 (2018), https://doi.org/10.1186/s40643-018-0215-7.
[65] X. Xu, J. Wang, R. Huang, W. Qi, R. Su, Z. He, Preparation of laccase mimicking nanozymes and their catalytic oxidation of phenolic pollutants, Catal. Sci. Technol. 11 (2021) 3402–3410, https://doi.org/10.1039/D1CY00074H.
[66] T. Phan-Xuan, B. Breitung, L.A. Dailey, Nanozymes for biomedical applications: multi-metallic systems may improve activity but at the cost of higher toxicity? Wiley Interdiscip. Rev. Nanomed. Nanobiotechnol. 16 (2024) e1981 https://doi.org/10.1002/WNAN.1981.
[67] C. Shang, Q. Wang, H. Tan, S. Lu, S. Wang, Q. Zhang, L. Gu, J. Li, E. Wang, S. Guo, Defective PtRuTe As nanozyme with selectively enhanced peroxidase-like activity, JACS Au 2 (2022) 2453–2459, https://doi.org/10.1021/JACSAU.2C00495/ASSET/IMAGES/LARGE/AU2C00495_0004.JPEG.
[68] Y. Wang, X. Gu, L. Zhao, D. Zhou, Nanozymes: an innovative approach to regulating heavy metal accumulation in plants and alleviating toxicity-A comprehensive review, Crit. Rev. Environ. Sci. Technol. (2024) 1–25, https://doi.org/10.1080/10643389.2024.2448048.
[69] X. Jin, C. Wu, X. Tian, P. Wang, Y. Zhou, J. Zuo, A magnetic-void-porous MnFe2O4/carbon microspheres nano-catalyst for catalytic ozonation: preparation, performance and mechanism, Environ. Sci. Ecotechnol. 7 (2021), https://doi.org/10.1016/j.ese.2021.100110.
[70] Z. Guan, Y. Guo, Z. Mo, S. Chen, J. Liang, X. Liao, Y. Zhang, Z. Huang, W. Song, Y. Xu, X. Ou, S. Sun, High-efficiency treatment of electroless nickel plating effluent using core-shell MnFe2O4-C@Al2O3 combined with ozonation: performance and mechanism, J. Hazard. Mater. 433 (2022), https://doi.org/10.1016/j.jhazmat.2022.128768.
[71] R.K. Sharma, R. Bandichhor, V. Mishra, S. Sharma, S. Yadav, S. Mehta, B. Arora, P. Rana, S. Dutta, K. Solanki, Advanced metal oxide-based nanocatalysts for the oxidative synthesis of fine chemicals, Mater. Adv. 4 (2023) 1795–1830, https://doi.org/10.1039/D2MA00977C.